PAN

Opto-Electronics Review

journal homepage: https://journals.pan.pl/opelre

Optical characteristics of *Portulaca grandiflora*-doped Cellulose using the spray pyrolysis technique

Tahseen Alaridhee*, Mohammed T. Obeed, Fatima H. Malk, Baheya A. Dhahi

Department of Material Science, Polymer Research Centre, University of Basrah, Iraq

Article info

Article history:
Received 19 Mar. 2023
Received in revised form 10 Jun. 2023
Accepted 21 Jun. 2023
Available on-line 19 Jul. 2023

Keywords:
Green materials;
optical properties;
natural dye;
biopolymer;
spray pyrolysis technique.

Abstract

Thin films were prepared based on cellulose polymer doped with different ratios of natural dye derived from *Portulaca grandiflora* concentrations. The polymer and natural dye were extracted from eco-friendly materials—the cell walls of millet husks and *Portulaca grandiflora*, respectively. The spray pyrolysis technique was applied to prepare thin film samples to control the film morphology and reduce the roughness of the surface. Optical microscope and Fourier transform infrared were used to analyse structural, morphological, and functional groups for all samples, respectively. The peak absorbance, extinction coefficient, optical bandgap, Urbach energy, and optical conductivity for the thin films were determined using ultraviolet-visible spectroscopy. The results show an enhancement in the optical characteristics when the natural cellulose is doped with a dye. Doping cellulose with 5% *P. grandiflora* has led to a considerable reduction in the energy bandgap (to 1.95 eV), compared to the sample doped with 1%.

1. Introduction

In recent years, there has been a growing interest in green renewable energy owing to its role in alleviating human and environmental health issues. Natural dye is increasingly a vital component of the world's green materials and sustainable development [1]. The most significant sources of natural dyes have been obtained from various sources, including insects, animals, minerals, and plants [2]. Since the early days of civilization, natural dyes have been used extensively in wear, fine art, and even medicine. Natural dyes are also safe to use and preserve ecological equilibrium [3–6]. Darkening materials with natural dyes have received increased attention from scientists and companies for their efficiency gains and environmental integrity. Several researchers have reported significant developments in pigment extraction from plant sources such as petals, flowers, leaves, seeds, and bark, resulting in increased extraction percentages [7, 8]. Natural dyes provide biomaterial pigments such as phycocyanin [9], chlorophyll [10, 11], luteolin, tannins [12, 13], violaxanthin [14, 15], and phycoerythrin [16, 17]. The technique for the extraction of natural dye has been covered extensively in the past, including reports on its use in dye-sensitized solar cells [18, 19], photosensitizers [20], and optoelectronic applications (optical sensors, optical interconnects, and medical equipment) [21–23].

However, the major challenge in the use of natural dyes for optoelectronic applications is their low electrical conductivity, which requires to be enhanced to improve their properties. It is crucial to research innovative development in materials that can increase the performance of semiconductors and optoelectronic devices. Efficient exciton creation is critical in photoelectronic systems, allowing for a narrow energy bandgap to shape [24, 25]. A combination of inorganic functional components and organic polymers can lead to synergistic qualities that have attracted considerable interest in literature. An interface made of a dye-doped polymer can offer improved absorption characteristics across an extensive range of wavelengths, making it an attractive material for specific applications [26, 27].

The modifications made by the polymer dopant are due to the improved electrical interaction between the dye electrolyte and the semiconducting electrode. The organic dye functions as a prototype model, while the polymer (cellulose [$C_6H_{10}O_5$]) acts as an electron acceptor molecule,

*Corresponding author at: tahseen.alaridhee@uobasra.edu.iq

https://doi.org/10.24425/opelre.2023.146553
1896-3757/ Association of Polish Electrical Engineers (SEP) and Polish Academic of Sciences (PAS). Published by PAS

facilitating the transfer of charge from the pigment to the electrode and enabling the system to function. Natural cellulose is considered the most common renewable polymer that has the potential to replace synthetic polymers in various applications [28, 29]. Cellulose has emerged as a critical element in developing advanced materials, particularly electroactive paper which has numerous potential applications in fields such as flexible electronics, sensing, and actuation.

Given these considerations, this work aims to analyse and describe the dye extracted from a natural source (*P. grandiflora*) which has been doped with natural cellulose. Figure 1 addresses the natural source used in this work as a green material. The study will discuss the effect of doping dye on the polymer and then examine its optical properties. The effect of the dopant dye on the cellulose is investigated using samples with various ratios of the dye and the cellulose. The latter is checked through morphological and structural studies using an optical microscope. The structure of the obtained additive has also been confirmed using the Fourier transform infrared (FTIR) spectroscopy.

Fig. 1. The green materials used in the extraction of *P. grandiflora* plant and cellulose from millet husks, respectively.

2. Experiment

2.1. Materials and equipment

The petals of the *P. grandiflora* plant were used to extract the dye. This plant is widespread in the private and public gardens in Basrah city in Iraq [see Fig. 1(a)]. The dye was extracted by using a magnetic stirring device (BOECO Hot Plate Magnetic Stirrer, model MSH 420, Boeco Germany, Germany). The magnetic stirrer has a maximum stirring capacity of 15 L, a stirring speed of 60–1110 rpm, and a heating surrounding temperature of 450 °C. Transmittance and absorbance spectra of thin films were carried out in a region of 350–900 nm using the GBC Cintra-2020 ultraviolet-visible (UV-VIS) spectrometer, (GBC, Australia). HD Microscope Camera ICC50 and DM500 microscope (Leica Microsystems, Germany) were used to analyse the surface image. The functional groups located in the samples were recorded using the Shimadzu IR Prestige 21 (Shimadzu Scientific Instruments, Japan), with the range of 200–4000 cm^{-1}.

2.2. Dye extraction process

Approximately 200 g of blossoms were gathered and their petals were subsequently cleaned to eliminate dust particles. After washing, the petals were placed at room temperature for ten days in a dark and dry setting before being pulverized in a crusher to create powder. The powdered product (1.5 g) was placed in a capped glass beaker with 50 ml of distilled water to obtain an aqueous extract. The mixture was then filtered using medium-fast filter paper, which weighed 55 g/m^2 and had a thickness of 0.33 mm. A 1:50 ratio of natural dye to water solvent was mixed, followed by magnetic stirring. The process inputs were adjusted at 50 °C with several rotations (200 rpm) for 40 min. The aqueous colour derived from the *P. grandiflora* flower is shown in Fig. 2(a).

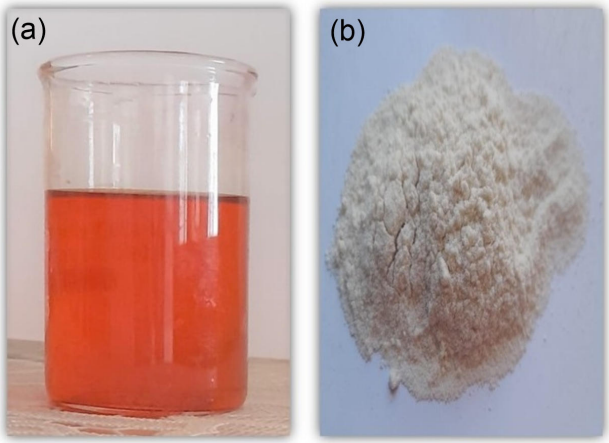

Fig. 2. The aspect of (a) extracted dye from *P. grandiflora* and (b) extracted cellulose from millet husks.

2.3. Extraction of cellulose

The natural polymer used in this work is cellulose, which is extracted from the cell walls of plants including millet husks [see Fig.1(b)]. The plant was collected and dirt or debris was removed, as well. The husks were then rinsed thoroughly to remove any remaining dirt or impurities. After that, the yields were placed in a container of water to allow soaking overnight, which helps to loosen the cellulose fibres and make them easier to extract. The husks were then ground into a fine powder using a grinder.

Cellulose fibres are separated from the husk debris, through acid hydrolysis, a chemical method which uses acid to dissolve the lignin and hemicellulose in the husk, leaving the cellulose fibres behind. Sulfuric acid is commonly used for acid hydrolysis of cellulose fibres and a concentration of 10% is used resulting in an acid solution at a temperature of 150 °C for 1 h. The cellulose fibres were thoroughly rinsed with water to remove any remaining impurities and were placed in a low-temperature oven for drying. Once the cellulose fibres were dry [see Fig. 2(b)], an airtight container was used to store the product.

2.4. Preparation of thin films

Figure 3 illustrates the setup of a homemade spray pyrolysis technique (SPT). The details of this technique are described in other works [30]. Electrical heaters were used to reach the desired temperature of the glass substrates. An adjustable variance thermostat was used to keep the substrate temperature at 75 ± 5 °C. A suitable quantity of dye composition (natural dye and water, 1:50 ratio) was stirred to produce an appropriate spraying solution employing carrier gas that contains pressurized nitrogen at 1.2 bar. The volumetric quantity with a dye content of 8%

was used as a spray solution. A spray volume of 25 ccs with the resulting solution was painted on the glass substrate for 30 min with one-minute intervals, given that each spray step takes 3 s. In the final step, all films were allowed to cool naturally to room temperature.

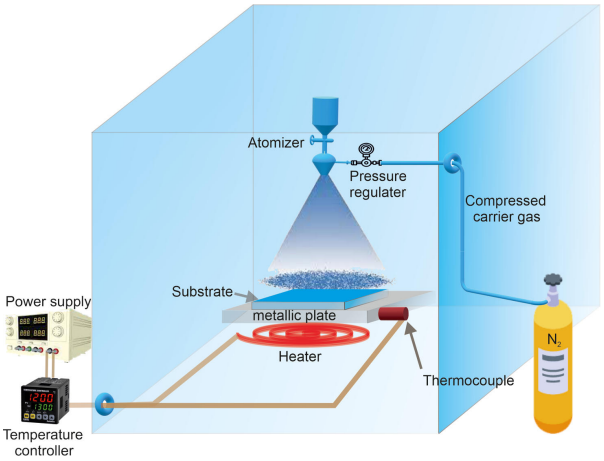

Fig. 3. Schematic view of the spray pyrolysis setup.

3. Characterisation

3.1. Optical microscope analysis

Enlarged images were captured using an optical microscope to better illustrate the morphological and structural characteristics of doped and pure samples. Slides were observed and photographs were taken with the DM500 microscope and the ICC50 HD camera, respectively (see Fig. 4). The photomicrographs of the slides were digitized using the Leica LAS EZ Software. The thin films with images of *P. grandiflora* reveal the shape, size, and distribution of the pigment particles, as well as the impurities that may be present in the sample. Figure 4(a) presents a good homogeneity and quality of the pigment dispersion in the film. The morphological characteristics of the polymer matrix (cellulose) with different concentrations of *P. grandiflora* dye are presented in Figs. 4(b), 4(c), and 4(d). These images depict the agglomeration of the pigment particles within the polymer matrix. As can be seen from Fig. 4, the samples were well prepared using the SPT. The pigment particles are well dispersed within the polymer matrix suggesting their homogeneous distribution throughout the film. Overall distribution and dispersion of the pigment particles in the matrix seem satisfactory, with minimal aggregation or deformation. The prepared samples are as close as possible to a uniform thickness for pure dye (261, 1044, 1058, and 1061 nm) and *P. grandiflora*-doped cellulose (PC) (1%, 3%, and 5%), respectively. The thickness values of the film were obtained using a standard approach that involves calculating the mass values of the glass substrate (m_1) and the dye layer (m_2) on the same surface as follows:

$$d = \frac{m_2 - m_1}{\rho\, a}. \qquad (1)$$

The parameters ρ and a represent the density of the dye and/or polymer and the area of the sample.

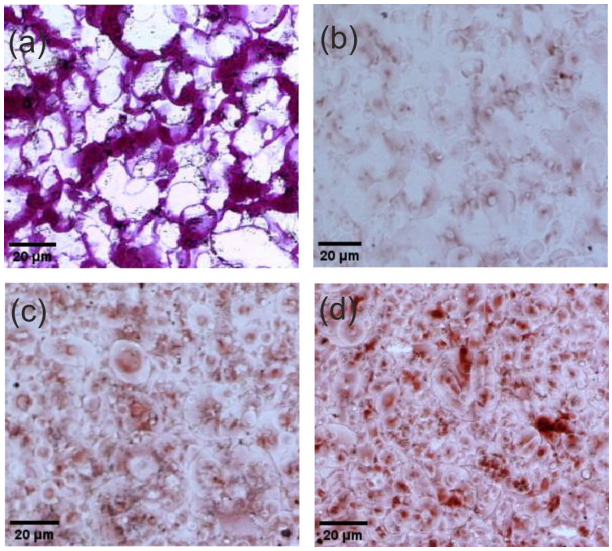

Fig. 4. Optical microscope image of (a) pure *P. grandiflora*, (b) PC 1%, (c) PC 3%, and (d) PC 5% at 20× magnification.

3.2. FTIR spectroscopy analysis

FTIR spectra of the powdered dye, natural cellulose, and dye-doped cellulose of different concentrations (1%, 3%, and 5%) were closely investigated to identify the composition and chemical interactions. In Fig. 5, the FTIR spectra of pure dye and natural cellulose were individually presented. The peaks that appeared at different frequencies are expressed in capital letters as listed in Table 1.

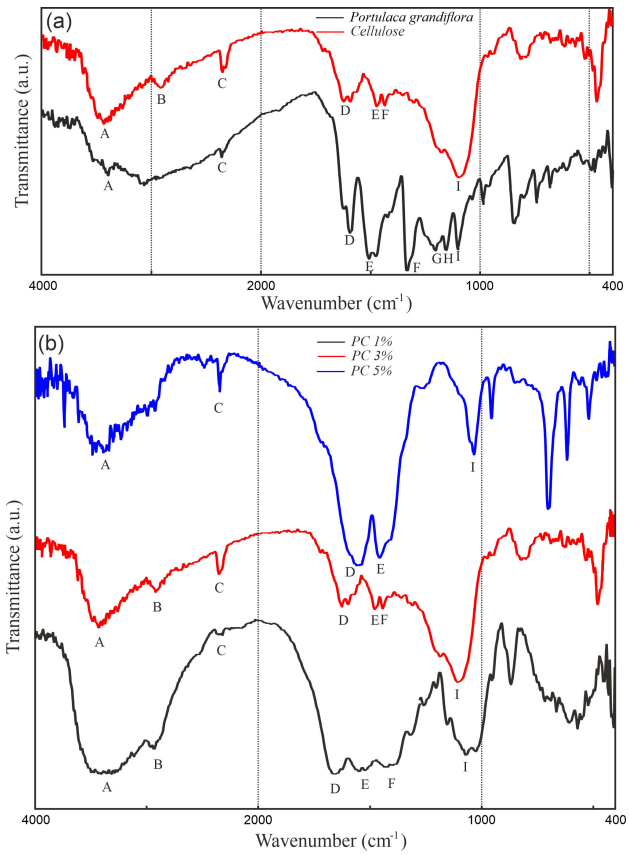

Fig. 4. FTIR spectroscopy of extracted (a) *P. grandiflora* plant, natural cellulose, and (b) different concentrations of dye-doped cellulose at room temperature.

Table 1.
Structural composition of natural dye, natural cellulose, and dye-doped cellulose from IR spectroscopy.

Peak	Pure dye		Cellulose		PC 1%		PC 3%		PC 5%	
	Wavenumber peak (cm^{-1})	Characteri-sation	Wavenumber peak (cm^{-1})	Characteri-sation	Wavenumber peak (cm^{-1})	Characteri-sation	Wavenumber peak (cm^{-1})	Characteri-sation	Wavenumber peak (cm^{-1})	Characteri-sation
A	3071	stretching ν O–H	3438	stretching ν O–H	3438	stretching ν O–H	3438	stretching ν O–H	3493	stretching ν O–H
B	--	--	2924	stretching aliphatic ν C–H	2924	stretching aliphatic ν C–H	2924	stretching aliphatic ν C–H	--	--
C	2342	stretching ν =C–H	2360	stretching ν –C≡C–	2360	stretching ν –C≡C–	2360	stretching ν –C≡C–	2359	stretching ν –C≡C–
D	1593	stretching aromatic ν C=C	1627	stretching carbonyl ν C=O	1627	stretching carbonyl ν C=O	1627	aromatic ν C=C	1563	stretching ν C–O
E	1510	aromatic ν C=C	1478	bending –CH_2 group	1478	bending –CH_2 group	1478	bending –CH_2 group	1458	--
F	1338	bending –CH_3 group	1441	bending –CH_2 group	1441	bending –CH_2 group	1441	bending –CH_2 group	--	--
G	1209	stretching ν C–O	--	--	--	--	--	--	--	--
H	1160	stretching ν C–O–C	--	--	--	--	--	--	--	--
I	1105	stretching ν C–O	1105	stretching ν C–O–C	1074	bending –CH_2 group	1105	bending –CH_3 group	1035	stretching ν C–C

The purpose of presenting the IR spectra of pure dye and the natural polymer is to identify the chemical bonds that occur in the substance. As can be seen from Fig. 5(a), the stretching mode in cellulose has strong absorption bands in the regions of 2900–3500 cm^{-1}, 1630–1620 cm^{-1}, and 1100–1150 cm^{-1}. On the other hand, the *P. grandiflora* typically exhibits absorption bands in the 1590–1580 cm^{-1} and 1340–1350 cm^{-1} ranges. In Fig. 5(b), the absorption bands from cellulose and *P. grandiflora* are combined in the IR spectrum. Cellulose dominates the overall shape of the spectrum, although there are additional absorption bands corresponding to the presence of *P. grandiflora* dye. In Fig. 5(b), all PC films show A, B, and C peaks, except the dye with 5% concentration, which has no peak at position B. These bands are due to the O–H, the aliphatic (ν C–H) stretching mode and stretching vibrations of the C≡C triple bond group, respectively. As can be seen from Fig. 5(b), the band D of PC 1%, PC 3%, and PC 5% corresponds to the carbonyl (ν C=O), aromatic (ν C=C), and ester (ν C–O) stretching frequencies, respectively. According to the stretching mode at E, the bending vibration in the spectrum of PC 3% is associated with the CH groups, while the band of PC 1% corresponds to C–H deformation vibration, and no mode is presented at that position for PC 5%. Furthermore, PC 5% displays stretching mode, which corresponds to the C–H out of the plane while both PC (1% and 3%) present ester C–O–C bending vibrations, respectively, where all modes are represented by the letter F. Further investigation showed that the band represented by the letter I demonstrated the vibrations of CH_2 and CH_3 groups, and C–C bonds for PC (5%, 3%, and 1%), respectively.

4. Results and discussion

4.1. UV-VIS spectroscopy

The UV-VIS spectra in the 200–1100 nm range were recorded using the CE-7200 double beam spectrometer. The absorption peaks for the natural cellulose, pure dye, and PC (1%, 3%, and 5%, respectively) thin films were located at 374, 450, 510, 511, and 512 nm, respectively. The UV absorption bands corresponded to the $\pi \rightarrow \pi^*$ electronic transitions of pigment components [31] [see Fig. 6(a)]. Furthermore, the absorption peaks of the doped samples shifted to the red region compared to the pure cellulose due to an increase in the amount of electron delocalization in the molecule. This leads to a decrease in the energy jump between highest occupied molecular orbital (HOMO) and lowest unoccupied molecular orbital (LUMO) [32].

Figure 6(b) shows the reflection patterns for both pure dye and dye-doped with different concentrations. Compared to pure dye, the presence of natural dye in all doped samples resulted in a considerable shift towards longer wavelengths in the reflection spectrum, indicating a redshift. This shift confirms the increase in the absorption of light by the dye. Table 1 shows the structural composition of natural dye, natural cellulose, and dye-doped cellulose from IR spectroscopy.

4.2. Bandgap and Urbach energy

HOMO-LUMO energy E_g is a crucial factor in determining semiconductor and dielectric properties. The optical bandgap denotes the creation of separate and

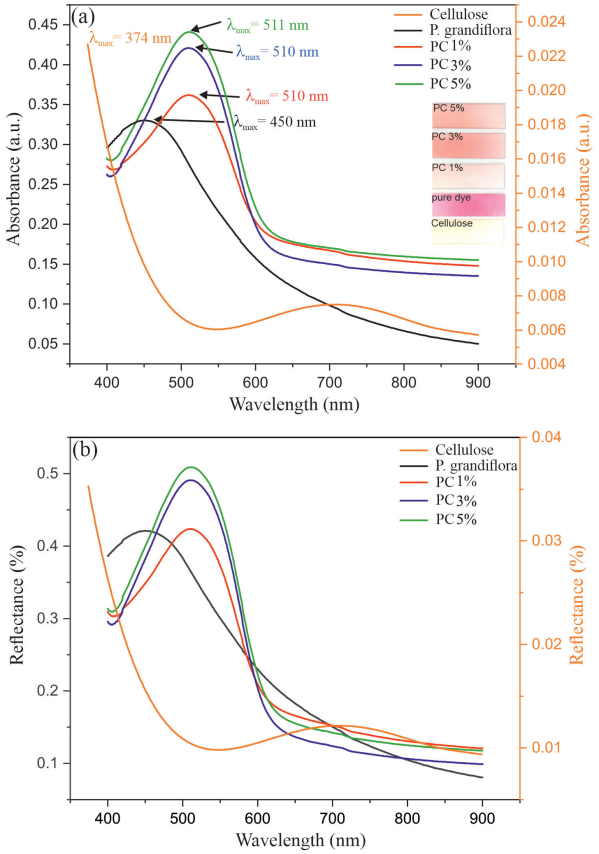

Fig. 6. The spectrum of UV-VIS (a) absorption and (b) reflection of pure dye, natural cellulose and different concentrations of dye-doped cellulose. Inset of Fig. 6(a) shows photographs of the pure dye, cellulose, and doped cellulose samples.

unconnected holes and free electrons with the lowest possible degree of energy. The determination of the optical bandgap using UV-VIS absorbance spectra was accomplished through the application of the Tauc relation as defined [33]

$$\alpha = \frac{\{h\nu - E_g\}^{\gamma}}{h\nu}. \tag{2}$$

Here, γ refers to the density distribution of the state index, which takes different values depending on the moment of transition: direct (1/2 and 3/2 for allowed and forbidden, respectively) or indirect (2 and 3 for allowed and forbidden, respectively). The intercept of $(\alpha h\nu)^{\gamma}$ against $(h\nu)$ with the x-axis is applied in this analysis to determine the energy gap values. The plots of $(\alpha h\nu)^{\gamma}$ *vs*. $(h\nu)$ were carried out for both direct and indirect transitions. As previously documented, the plot for direct transition shows a perfect fit, while the plot for indirect transition exhibits a less perfect fit in extrapolation [34]. This leads to the understanding that a direct bandgap transition would be more useful in photovoltaic systems.

Figures 7(a), 7(b), 7(c), 7(d) present the Tauc plots for direct bandgap transition. Figure 7(a) presents the values of E_g for natural dye and cellulose. As expected, the E_g of pure dye is lower than that found in cellulose. As dye concentration increases, the values of the direct optical bandgap for the doped samples decrease. The electronic properties of the dye-doped polymer samples are also affected by the type of dye, the polymer matrix, and the processing conditions. The effect of dye-doped cellulose on the Urbach energy is illustrated in Fig. 8. It is well known that Urbach energy is a measure of the disorder in the electronic band structure of a material. Greater Urbach

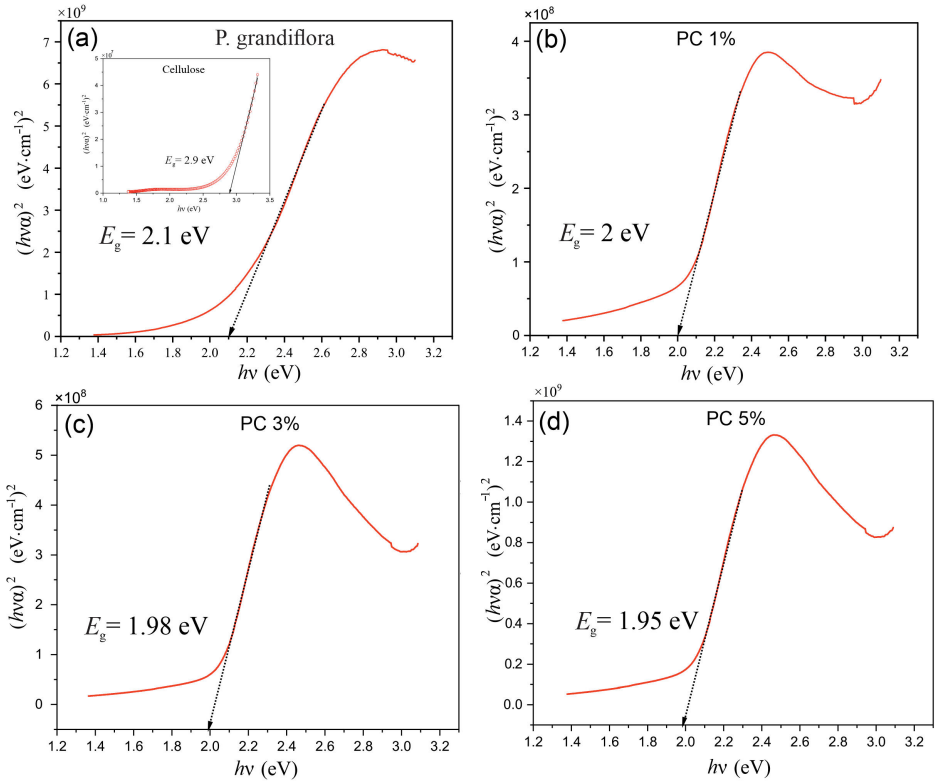

Fig. 7. Energy bandgap of (a) pure dye, (b) PC 1%, (c) PC 3%, and (d) PC 5%. Inset of Fig. 7(a) shows energy bandgap of natural cellulose.

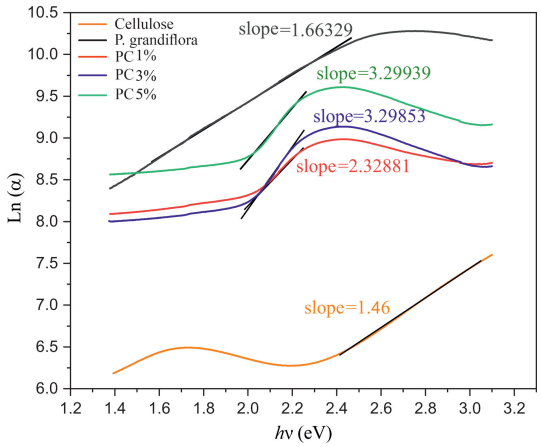

Fig. 8. Estimation of Urbach energy for pure dye, cellulose, and dye-doped cellulose in different ratios of concentrations using the graphical slope of photon energy *vs*. ln α.

energy causes more disturbances because of inadequate crystalline or amorphous solid structures [35, 36]. The values of the direct energy gap and Urbach tail for each sample are outlined in Table 2. As can be seen from Fig. 8, the tail energy is influenced by doping with impurities. The energy-correlated defect bands has a minimum value as the dye concertation is increased. Typically, larger dye molecules occupy more volume compared to the polymer chains, leading to more restrictions in their movement. This leads to a more ordered arrangement of the polymer chains, reducing structural disorder.

Table 2.
The values of energy gaps with Urbach tails for the pure and doped samples.

Sample	Direct band gap (eV)	Urbach tail (eV)
Cellulose	2.90	0.685
Pure dye	2.10	0.601
PC 1%	2.00	0.429
PC 3%	1.98	0.303
PC 5%	1.95	0.303

4.3. Refractive index and extinction coefficient

The refractive index (n) and extinction coefficient (k) of pure dye and dye-doped polymer are demonstrated, respectively, in Figs. 9(a) and 9(b). The factors n and k are expressed in terms of a complex relation, which can be written as

$$N(\lambda) = n(\lambda) + ik(\lambda). \tag{3}$$

The real part n and imaginary part k of the pure dye, cellulose, and PC (1%, 3%, and 5%) thin films were estimated using the two relations as follows [37]:

$$n = \frac{1+R}{1-R} + \sqrt{\frac{4R}{(1-R)^2} - k^2}, \tag{4}$$

$$k = \frac{\alpha\lambda}{4\pi}, \tag{5}$$

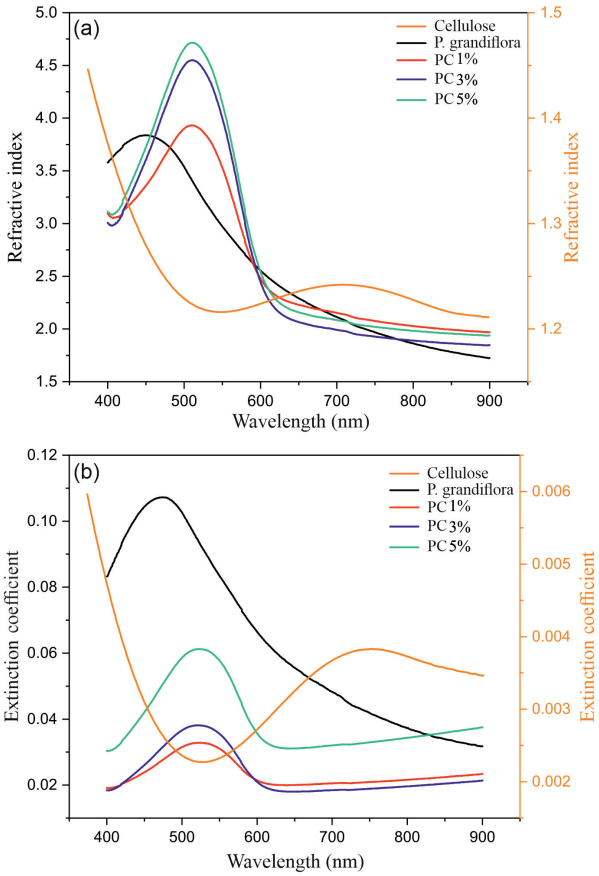

Fig. 9. (a) Refractive index and (b) extinction coefficient *vs*. wavelength of pure dye, cellulose, and different concentrations of dye-doped cellulose.

where R is the reflectance spectra and α the absorption coefficient. As the dopant concentration of the *P. grandiflora* increases, it leads to a rise in the refractive index of the dye-doped polymer [see Fig. 9(a)]. This is due to the light scattering by the dye molecules, resulting in more light being bent as it passes through the material. In Fig. 9(b), the presence of the dye in cellulose slows down the absorption process which leads to an increase in the extinction coefficient of the doped samples as the *P. grandiflora* concentration ratios increase.

4.4. The complex dielectric constant and optical conductiviy

An associated feature of a substance is its complex dielectric constant, expressed as $\varepsilon = \varepsilon_r + \varepsilon_i$, which gives additional insight into its optical properties. The real and imaginary parts of the dielectric function are calculated as [38]:

$$\varepsilon_r = n^2 - k^2 \tag{6}$$

$$\varepsilon_i = 2nk. \tag{7}$$

The ability of a material to store electromagnetic waves is described, in portion, by the real part of the dielectric function, along with the imaginary part. The behaviour of the dielectric function ε_r and ε_i *vs*. the wavelength is demonstrated in Figs. 10(a) and 10(b), respectively. Figure 10(a) depicts that the doped thin films have a high refractive index at a wavelength of 510 nm compared to

that of cellulose. This finding is indicated by the high value of ε_r, as shown in Fig. 9(a). In the blue region, ε_r increases as the dye concentration increases, which means the substance becomes more polarized in response to an electric field. The imaginary part of the dielectric function also describes the absorption of light by a material. For the doped samples, there is considerable absorption in the blue region in contrast to the cellulose, which exhibits slight absorption in the UV region. As the dye concentration ratio increases, the value of ε_i increases noticeably, indicating that the material has a high optical absorption [see Fig. 10(b)].

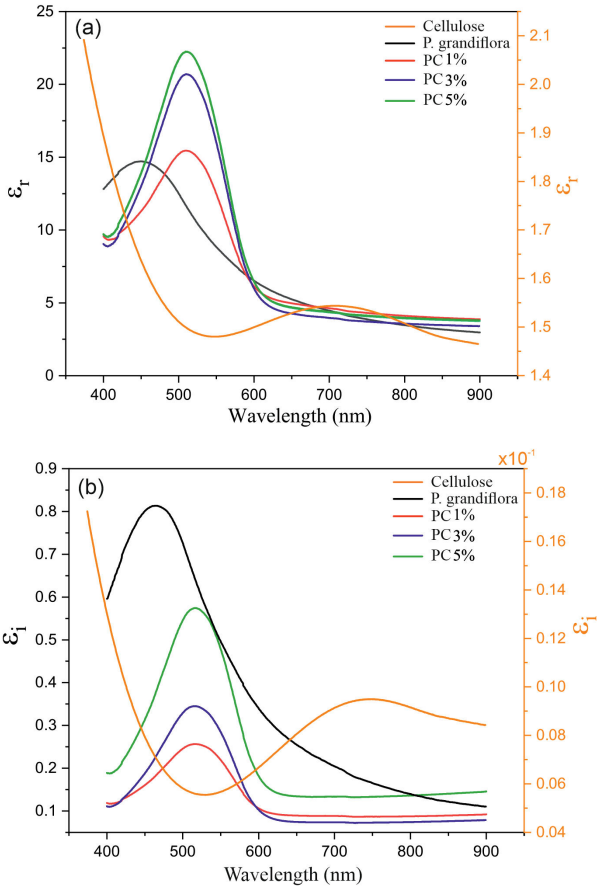

Fig. 10. (a) Real and (b) imaginary parts of the dielectric function for pure dye, cellulose, and different concentrations of dye-doped cellulose.

The fundamental property in various applications such as photovoltaics and photonics is complex optical conductivity. The latter can support designing a thin film of new material with desired optical and electrical properties. The optical conductivity was calculated using the following equations [38]

$$\sigma_r = \omega \varepsilon_0 \varepsilon_i \tag{8}$$

$$\sigma_i = \omega \varepsilon_0 \varepsilon_r. \tag{9}$$

The real part σ_r and imaginary part σ_i *vs.* wavelength are presented in Figs. 11(a) and 11(b), respectively. From Fig. 11(a), in the blue region, the real part σ_r becomes more effective with increasing dye concentration ratios with respect to that of cellulose. This means that the sample ability of a material to conduct electricity becomes greater.

On the other hand, the imaginary part of optical conductivity in the blue region shows an increase in the material conductivity, as the dye concentration ratios increase [see Fig. 11(b)]. This increase is mainly due to light absorption, which appears in the behaviour of the extinction coefficient shown in Fig. 9(b).

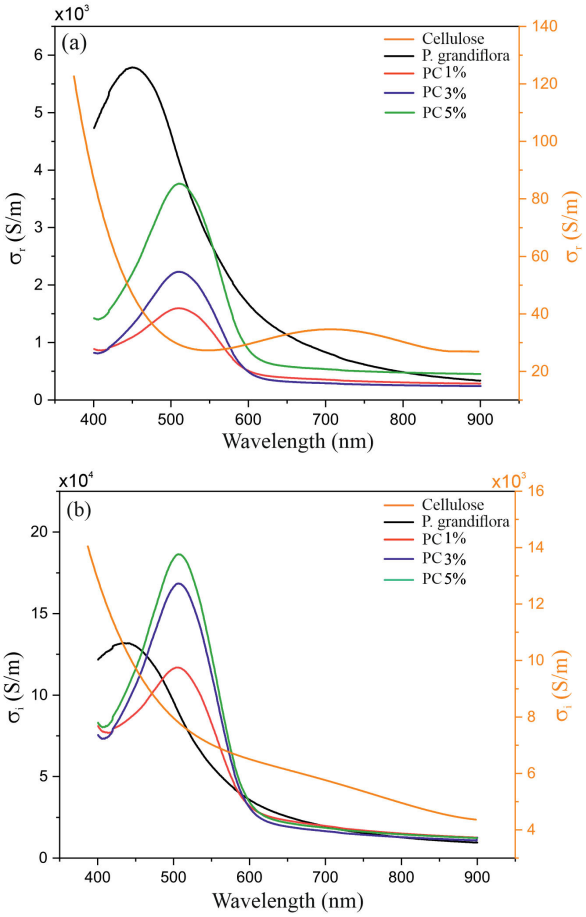

Fig. 11. (a) Real and (b) imaginary parts of the optical conductivity for pure dye, cellulose and different concentrations of dye doped cellulose.

5. Conclusions

Pigment extracted from *P. grandiflora* is utilized as a natural dye source for producing cellulose thin films doped with varying dye concentrations via the SPT. This latter technique allows for obtaining thin film samples with a coating layer of high uniformity and homogeneity. The UV-VIS and FTIR spectra demonstrate the effectiveness of using dye molecules as dopants to enhance the linear optical characteristics of cellulose films. The proportion of dopant concentration affects the refractive index and extinction coefficient of dye-doped polymer films. Once the dopant concentration reaches 5%, the material exhibits a direct energy gap of 1.95 eV. The study of the dielectric function and the optical conductivity indicates that the prepared samples exhibit significant responses to electric energy. The presence of natural dyes in the biopolymer (cellulose) enhances the ability of the doped samples to interact and absorb light, demonstrating them as cost-effective and eco-friendly choices for dye-based photovoltaic applications.

Authors' statement

T.A. performed the data analysis, interpretation, writing, and gave final approval of the article. M.T.O. conducted the sample coating using the SPT, collected and/or assembled the data, and critically revised the article. F.H.M. carried out the dye/cellulose extraction and sample preparation. B.A.D. conducted the UV and IR measurements.

Acknowledgements

This work was partially supported by the Polymer Research Center (PRC) at the University of Basrah by providing the researchers with the necessary examinations and laboratory equipment.

References

[1] Shahid, M., Shahid-ul-Islam & Mohammad, F. Recent advancements in natural dye applications: a review. *J. Clean. Prod.* **53**, 310–331 (2013). https://doi.org/10.1016/j.jclepro.2013.03.031

[2] Yusuf, M., Shabbir, M. & Mohammad, F. Natural colorants: historical, processing and sustainable prospects. *Nat. Prod. Bioprospect.* **7**, 123–145 (2017). https://doi.org/10.1007/s13659-017-0119-9

[3] Patterson, K. A., Grimm, C. M. & Corsi, T. M. Adopting new technologies for supply chain management. *Transp. Res. E: Logist. Transp.* **39**, 95–121 (2003). https://doi.org/10.1016/S1366-5545(02)00041-8

[4] Sarkis, J., Meade, L. M. & Talluri, S. E-logistics and the natural environment. *Supply Chain Manag*. **9**, 303–312 (2004). https://doi.org/10.1108/13598540410550055

[5] Fulekar, M. H. Bioremediation technology for hazardous wastes-recent advances. in *Bioremediation Technology* (ed. Fulekar, M H.) 135–166 (Springer Netherlands, 2010). https://doi.org/10.1007/978-90-481-3678-0_5

[6] Kasiri, M. B. & Safapour, S. Natural dyes and antimicrobials for green treatment of textiles. *Environ. Chem. Lett*. **12**, 1–13 (2014). https://doi.org/10.1007/s10311-013-0426-2

[7] Mortensen, A. Carotenoids and other pigments as natural colorants. *Pure Appl. Chem*. **78**, 1477–1491 (2006). https://doi.org/10.1351/pac200678081477

[8] Kalra, R., Conlan, X. A. & Goel, M. Fungi as a potential source of pigments: harnessing filamentous fungi. *Front. Chem*. **8**, 369 (2020). https://doi.org/10.3389/fchem.2020.00369

[9] Zheng, J. & He, L. Surface-enhanced Raman spectroscopy for the chemical analysis of food. *Compr. Rev. Food Sci. Food Saf*. **13**, 317–328 (2014). https://doi.org/10.1111/1541-4337.12062

[10] Feret, J.-B. *et al*. PROSPECT-4 and 5: Advances in the leaf optical properties model separating photosynthetic pigments. *Remote Sens. Environ.* **112**, 3030–3043 (2008). https://doi.org/10.1016/j.rse.2008.02.012

[11] Balusamy, S. R. *et al*. Chitosan, chitosan nanoparticles and modified chitosan biomaterials, a potential tool to combat salinity stress in plants. *Carbohydr. Polym*. **284**, 119189 (2022). https://doi.org/10.1016/j.carbpol.2022.119189

[12] Alaridhee, T. A., Malk, F. H., Hussein, A. A. & Abid, D. S. Enhanced absorption edge of Anchusa-Italica-doped pentacene towards optoelectronic applications. in *Current Advances in Materials Applications* (eds. Dahham, O & Zulkepli, N. N.) 251–263 (Trans Tech Publications, 2020). https://doi.org/10.4028/www.scientific.net/MSF.1002.251

[13] Baldwin, A. & Booth, B. W. Biomedical applications of tannic acid. *J. Biomater. Appl*. **36**, 1503–1523 (2022). https://doi.org/10.1177/08853282211058099

[14] Bouchouit, K. *et al*. Nonlinear optical properties of selected natural pigments extracted from spinach: Carotenoids. *Dyes Pigm.* **86**, 161–165 (2010). https://doi.org/10.1016/j.dyepig.2009.12.013

[15] Jacquemoud, S. & Ustin, S. *Leaf optical properties*. (Cambridge University Press, 2019).

[16] Anwer, K. *et al*. Role of N-terminal residues on folding and stability of C-phycoerythrin: simulation and urea-induced denaturation studies. *J. Biomol. Struct. Dyn.* **33**, 121–133 (2015). https://doi.org/10.1080/07391102.2013.855144

[17] Gonzalez-Ramirez, E. *et al*. Thermal and pH stability of the B-phycoerythrin from the red algae *Porphyridium cruentum*. *Food Biophys*. **9**, 184–192 (2014). https://doi.org/10.1007/s11483-014-9331-x

[18] Hagfeldt, A., Boschloo, G., Sun, L., Kloo, L. & Pettersson, H. Dye-sensitized solar cells. *Chem. Rev.* **110**, 6595–6663 (2010). https://doi.org/10.1021/cr900356p

[19] Grätzel, M. Dye-sensitized solar cells. *J. Photochem. Photobiol. C* **4**, 145–153 (2003). https://doi.org/10.1016/S1389-5567(03)00026-1

[20] Abrahamse, H. & Hamblin, M. R. New photosensitizers for photodynamic therapy. *Biochem. J.* **473**, 347–364 (2016). https://doi.org/10.1042/BJ20150942

[21] Askim, J. R., Mahmoudi, M. & Suslick, K. S. Optical sensor arrays for chemical sensing: the optoelectronic nose. *Chem. Soc. Rev.* **42**, 8649–8682 (2013). https://doi.org/10.1039/C3CS60179J

[22] Miller, D. A. Device requirements for optical interconnects to silicon chips. *Proc. IEEE Inst. Electr. Electron. Eng.* **97**, 1166–1185 (2009). https://doi.org/10.1109/JPROC.2009.2014298

[23] Improta, G., Perrone, A., Russo, M. A. & Triassi, M. Health technology assessment (HTA) of optoelectronic biosensors for oncology by analytic hierarchy process (AHP) and Likert scale. *BMC Med. Res. Methodol.* **19**, 140 (2019). https://doi.org/10.1186/s12874-019-0775-z

[24] Graetzel, M., Janssen, R. A., Mitzi, D. B. & Sargent, E. H. Materials interface engineering for solution-processed photovoltaics. *Nature* **488**, 304–312 (2012). https://doi.org/10.1038/nature11476

[25] Miyata, A. *et al*. Direct measurement of the exciton binding energy and effective masses for charge carriers in organic–inorganic tri-halide perovskites. *Nat. Phys.* **11**, 582–587 (2015). https://doi.org/10.1038/nphys3357

[26] Samuel, I. D. W. & Turnbull, G. A. Organic semiconductor lasers. *Chem. Rev*. **107**, 1272–1295 (2007). https://doi.org/10.1021/cr050152i

[27] Kim, M. *et al*. Fabrication of microcapsules for dye-doped polymer-dispersed liquid crystal-based smart windows. *ACS Appl. Mater. Interfaces* **7**, 17904–17909 (2015). https://doi.org/10.1021/acsami.5b04496

[28] Yu, L., Dean, K. & Li, L. Polymer blends and composites from renewable resources. *Prog. Polym. Sci.* **31**, 576–602 (2006). https://doi.org/10.1016/j.progpolymsci.2006.03.002

[29] Tabasum, S. *et al*. A review on blending of corn starch with natural and synthetic polymers, and inorganic nanoparticles with mathematical modeling. *Int. J. Biol. Macromol.* **122**, 969996 (2019). https://doi.org/10.1016/j.ijbiomac.2018.10.092

[30] Obeed, M. T. Study of the optical and electrical properties of melanin pigment. (University of Basrah, 2013).

[31] Sutherland, R. L. *Handbook of Nonlinear Optics*. (CRC Press, 2003). https://doi.org/10.1201/9780203912539

[32] Prima, E. C., Hidayat, N. N., Yuliarto, B. & Dipojono, H. K. A combined spectroscopic and TDDFT study of natural dyes extracted from fruit peels of *Citrus reticulata* and *Musa acuminata* for dye-sensitized solar cells. *Spectrochim. Acta A Mol. Biomol. Spectrosc.* **171**, 112–125 (2017). https://doi.org/10.1016/j.saa.2016.07.024

[33] Tauc, J. & Menth, A. States in the gap. *J. Non Cryst. Solids* **8**, 569–585 (1972). https://doi.org/10.1016/0022-3093(72)90194-9

[34] Reddy, K. M., Manorama, S. V. & Reddy, A. R. Bandgap studies on anatase titanium dioxide nanoparticles. *Mater. Chem. Phys.* **78**, 239–245(2003). https://doi.org/10.1016/S0254-0584(02)00343-7

[35] Duan, L. *et al*. Comparative study of light-and thermal-induced degradation for both fullerene and non-fullerene-based organic solar cells. *Sustain. Energy Fuels* **3**, 723–735 (2019). https://doi.org/10.1039/C8SE00567B

[36] Ugur, E. *et al*. Life on the Urbach Edge. *J. Phys. Chem. Lett*. **13**, 7702–7711 (2022). https://doi.org/10.1021/acs.jpclett.2c01812

[37] Palik, E. D. *Handbook of Optical Constants of Solids, Third Edition* (Academic Press, 1998).

[38] Wakai, C., Oleinikova, A., Ott, M. & Weingärtner, H. How polar are ionic liquids? Determination of the static dielectric constant of an imidazolium-based ionic liquid by microwave dielectric spectroscopy. *J. Phys. Chem. B* **109**, 17028–17030 (2005). https://doi.org/10.1021/jp053946